

Desertification assessments in the Hexi corridor of northern China's Gansu Province by remote sensing

Lanying Han · Zhengcai Zhang · Qiang Zhang · Xin Wan

Received: 4 May 2014 / Accepted: 24 September 2014 / Published online: 8 October 2014
© Springer Science+Business Media Dordrecht 2014

Abstract The Hexi corridor region lies in the arid and semiarid regions of Gansu Province, China. The sensitive ecological environment has undergone severe desertification caused by natural environmental change and unsustainable exploitation of the region. Remote sensing and GIS are being used to study desertification in this region. In this paper, we used Landsat TM and HJ data between June and August in 2000, 2005, and 2010 to analyze the spatial and temporal patterns of the desertification using five indices: the modified soil-adjusted vegetation index, fractional vegetation cover, the surface albedo, land surface temperature, and the temperature–vegetation drought index. We normalized the indicators, determined their weights, and defined five grades of desertification: none, light, moderate, severe, and extremely severe. We found that desertification in the Hexi corridor covered more than 76 % of the total land area; the total area of desertified land was 22.02×10^4 , 21.22×10^4 , and 21.06×10^4 km² in 2000, 2005, and 2010, respectively, which amounted to 79.8, 76.9, and 76.3 % of the total area. In both periods, the most spatial changes in desertification showed a stability or reversal of desertification from 2000 to 2005 and from 2005 to 2010. From 2000 to 2010, the area in which desertification reversed (1.00×10^4 km²) was a little more than the area of newly desertified land

Electronic supplementary material The online version of this article (doi:[10.1007/s11069-014-1457-0](https://doi.org/10.1007/s11069-014-1457-0)) contains supplementary material, which is available to authorized users.

L. Han · Q. Zhang

Institute of Arid Meteorology, China Meteorological Administration (CMA), Key Open Laboratory of Arid Climatic Change and Reducing Disaster of CMA, Key Laboratory of Arid Climatic Change and Reducing Disaster, Lanzhou 730020, Gansu, People's Republic of China
e-mail: sthan07@hotmail.com

L. Han · X. Wan

Northwest Regional Climate Center, Lanzhou 730000, Gansu, People's Republic of China

Z. Zhang (✉)

Cold and Arid Regions Environmental and Engineering Research Institute, Chinese Academy of Sciences, No. 260, West Donggang Road, Lanzhou 730000, Gansu, People's Republic of China
e-mail: zhangzhsi@sina.com; zbdong@ns.lzb.ac.cn

($0.96 \times 10^4 \text{ km}^2$). The reversal of desertification mainly involved a change from severely and moderately desertified land to non-desertified land. Natural factor and human activity controlled the desertification process, but the reversal of desertification mainly resulted from human activity.

Keywords Hexi corridor · Desertification · Climate change · Human activity

1 Introduction

Desertification has been defined as land degradation in arid, semiarid, and dry sub-humid areas as a result of various factors, including climatic change and human activities (UNCCD 1994). Globally, the total area of desertified land in 1996 amounted to $3.6 \times 10^7 \text{ km}^2$, amounting to 24.1 % of Earth's land surface, and this affected on one-sixth of the world's population, most of whom live in poverty (Middleton and Thomas 1997). China is one of the countries which has been most seriously affected by desertification (Wang and Zhu 2003); the area of desertified land totaled $1.84 \times 10^7 \text{ km}^2$ in 2005, distributed across 13 provinces in northwestern, northern, and northeastern China (CCICCD 2006).

Desertification is driven by several interconnected factors and triggered by the combination of the natural predisposition of the environment with human pressures and climate change (UNCCD 1994; Adamo and Crews-Meyer 2006). In general, climatic conditions are the dominant drivers of desertification in northern China (Wang et al. 2008; Han 2003). Specific temperature, drought, and wind regime trends have been associated with desertification in China (Wang et al. 2006, 2008). However, human activities such as inappropriate and unsustainable land use are the main cause of sandy desertification in some regions (Ge et al. 2013). As these previous results indicate, the relative roles and synergistic effects of climate conditions and human activities on desertification are still not clear. Recently, researchers have tried to clarify the relationships among these factors and the resulting impacts on desertification (Luo et al. 2005; Xu et al. 2011; Ge et al. 2013).

Desertification mainly occurs in dry lands (e.g., Dregne et al. 1991; Kassas 1995; Sivakumar 2007), but it was affected by a wide variety of environments, climates, and societies (e.g., Arnalds 2004). Different methods have been used to analyze desertification. These include empirical approaches (e.g., Liu et al. 2003; Geist and Lambin 2004), remote-sensing applications (e.g., Liu and Wang 2007; Shalaby and Tateishi 2007; Zhang et al. 2008; Hu et al. 2012; Li et al. 2013; Xue et al. 2013), and modeling (e.g., Salvati et al. 2008; Ding et al. 2009).

With the development of remote-sensing technology, especially when combined with geographic information systems (GIS) technology, researchers now have an effective method for conducting desertification research for large areas (Wang et al. 1998; Hu et al. 2012). By analyzing remote-sensing imagery over a long time period, it becomes possible to assess desertification trends accurately and in a timely manner, thereby supporting the prediction and management of this problem.

The Hexi region lies in Gansu Province of northeastern China. It is an arid to semiarid region and has one of the most sensitive ecological environments and most severe desertification in China (Han et al. 2013). The problems that have developed in this region have attracted the attention of China's Central Committee and State Council, leading to

Table 1 Area of desertified land in study region in different periods

Study	Periods	Area ($\times 10^4$ km ²)	Proportion of area (%)		Desertification type
			Desertification developed	Desertification reversed	
Zhu and Liu (1989)	1989	5.60	–	–	–
Gao et al. (2001)	2000	21.3	75.3	0.38	Water erosion, wind erosion, and salinization
Wang (2003)	2003	5.03	18.25	–	–
Wang et al. (2005)	1994–2004	11.75	97.63	–	Wind erosion
Shi et al. (2006)	1999–2004	19.35	77.71	–0.21	Water erosion, wind erosion, and salinization

much research on this region. Table 1 summarizes recent studies of the desertification that has occurred in the Hexi region. The area of desertification in the Hexi region varies among studies (Zhu and Liu 1989; Gao et al. 2001; Wang 2003; Wang et al. 2005; Shi et al. 2006) due to differences in the research methods and changes in the area of desertification over time. Differences in the indicators used to assess desertification were also responsible. Previous research mostly focused on the use of a single indicator or of the relationship between a small number of indicators (Nasrallah and Balling 1993; Dall-Olmo and Karnieli 2002; Niu 2005; Zeng et al. 2006; Ma and Xiao 2007; Zeng and Feng 2007).

In this paper, we used Landsat TM and HJ-1A/B data obtained between June and August in 2000, 2005, and 2010 to analyze the spatial and temporal trends in desertification in the Hexi corridor. Satellite monitoring provides a rapid, frequent, and relatively inexpensive way to monitor such changes. The HJ-1A and 1B satellites are small Chinese Earth observation satellites that were launched on September 6, 2008. Among the payloads aboard these two satellites, their multispectral CCD cameras are important instruments that are widely used in eco-environmental monitoring. Each satellite carries two CCD cameras (CCD1 and CCD2), with a swath width of 700 km, a spatial resolution of 3,100 m, and a 48-h return period. The HJ-1A/1B CCDs have three visible bands (430–520, 520–600, and 630–690 nm) and one near-IR band (760–900 nm) (Wang et al. 2010; Sun et al. 2010). The satellite constellation is composed of three small satellites, supported by ground and application systems. It provides all-weather imagery. The two-satellite 1A and 1B constellation represents the first disaster monitoring spacecraft orbited by China.

We used five indicators in our analysis to assess the severity of desertification: the modified soil-adjusted vegetation index (MSAVI), surface albedo, land surface temperature (LST), fractional vegetation cover (FVC), and temperature–vegetation drought index (TVDI). Through comparisons of the five indicators and field investigations, we determined weights for the indicators and used them to define criteria for grading the severity of desertification. We also collected data on sandstorm frequency, temperature, relative humidity, and precipitation to analyze the influence of these factors on desertification. Simultaneously, to determine the effects of human activity on the desertification process, we analyzed the population, vegetation cover, cultivated land, and livestock. The results will help managers to assess regional desertification trends and develop more effective policies to combat desertification, changes in the regional ecological environment, and changes in the human environment.

2 Materials and methods

2.1 Study region

The Hexi corridor includes four cities: Zhangye, Jiuquan, Wuwei, and Dunhuang (Fig. 1). The corridor is bordered by the Tengger Desert in the east, the Badain Jaran Desert in the northeast, the Kumtagh Desert to the northwest, and the Qinghai-Tibetan Plateau to the southwest. It extends 800 km from east to west direction and 40–100 km from north to south (Gao et al. 2001). This region is far from the nearest sea, so there is little precipitation (an average annual total ranging from 50 to 200 mm), high temperatures (an annual average of 5–10 °C, with mean monthly values ranging from a minimum of −16 °C in January to a maximum of 27 °C in July), and strong evaporation, with pan evaporation averaging 2,000 mm annually (Ma et al. 2005). There are three continental rivers in the region: the Shiyang river, Heihe river, and Shulehe rivers in the eastern, middle, and western parts of the region (Fig. 1). The main types of desertified land are sand dunes (including mobile, semi-fixed, and fixed), wind-eroded land, saline and alkaline land, and water-eroded land (Wang 2003). Sand dunes and the desertified area are mainly found in the relatively flat land between Qilian Mountains in the south and the deserts to the north.

2.2 Indicators of desertification

As noted earlier, we used five indicators for the degree of desertification: MSAVI (Li and Zhou 2001), surface albedo (Nasrallah and Balling 1993; Wang et al. 2013a, b; Zeng et al. 2006), LST (Han et al. 2014; Luo et al. 2010; Ma and Xiao 2007), FVC (Han et al. 2014;

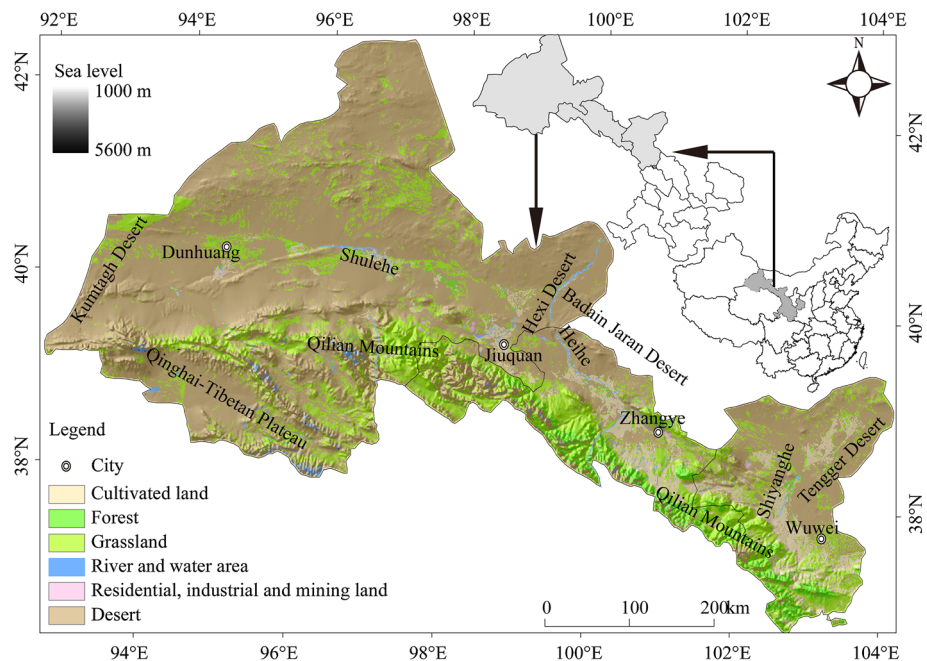


Fig. 1 Location of the Hexi region

Table 2 Indicators of desertification used to determine the degree of desertification

Degree	Indicator				
	MSAVI	FVC	Albedo	LST	TVDI
None	>1.0	>0.45	<0.65	<0.84	<0.50
Slight	0.75	0.35	0.73	0.86	0.57
Moderate	0.50	0.20	0.92	0.95	0.60
Severe	0.40	0.08	1.00	1.00	0.67
Extremely severe	<0.40	<0.08	>1.00	>1.00	>0.67
Weight	0.30	0.25	0.20	0.15	0.10

MSAVI modified soil-adjusted vegetation index, *FVC* fractional vegetation cover, *albedo* the surface albedo, *LST* land surface temperature, *TVDI* temperature–vegetation drought index

Wang et al. 2013a, b), and TVDI (Han et al. 2014; Li et al. 2008). We used maximum difference normalization method to normalize the value of each indicator, eliminate the subindex dimensional effects, weigh each indicator based on the average of the opinions of five experts (Table 2), and superimposing calculate the weighted five indexes, and used natural breaks (Jenks) classification method values to determine the degree of desertification by ArcGIS soft, and the natural breaks are based on natural groupings inherent in the data. ArcGIS identifies break points by picking the class breaks that best group similar values and maximizes the differences between classes. The features are divided into classes whose boundaries are set where there are relatively big jumps in the data values. To improve the accuracy of our monitoring, we used the same training samples. The data used to calculate the indicators were obtained by inversion of the same Landsat TM and HJ data with a spatial resolution of 30 m from 2000, 2005, and 2010, respectively. MSAVI had the highest precision and expressed the most information about desertification, followed by FVC, LST, Albedo, and TVDI (Table 3).

2.3 Data acquisition, processing, and analysis

The Landsat images were obtained from the Global Land Cover Facility (<http://glcfapp.umiacs.umd.edu/>), and HJ-1A/B obtained from the satellite Environment Center Ministry of Environmental Protection (<http://www.secmep.cn/secPortal/portal/index.faces>). Because images acquired in different seasons will have different properties, and because this can influence the desertification monitoring results, we chose a single season for all of the data. According to previous research results, late summer is the best season for monitoring desertification in northern China (Wu 2001a, b). In the different period, remote-sensing image calculation processes, using the histogram equalization method to nonlinear expanding the three period images, make the pixel numbers in a given gray value are equal for each image. Finally, the images are enhanced.

The images were processed by a data supply agency, including systematic geometric correction and radiometric calibration. The data were geo-referenced by using ground control points collected in the field around the study site and based on 1:50,000 scale topographic maps provided by Gansu Province bureau of surveying and mapping (<http://www.cehuiju.gansu.gov.cn/>). The correction accuracy was better than 1 pixel. The resulting data were projected using an Albers equal-area conic coordinate system. All the images were of high quality (with <10 % cloud cover). The images were atmospherically

Table 3 Classification precision of different combination of desertification monitoring indexes

One indicator	Classification precision				
	MSAVI	Albedo	LST	FVC	TVDI
Classification precision (%)	68.91	56.24	43.56	66.84	30.57
Two indicators	MSAVI + Albedo	MSAVI + LST	MSAVI + TVDI	FVC + Albedo	FVC + LST
Classification precision (%)	86.59	84.63	77.65	85.31	82.49
Three indicators	MSAVI + Albedo + LST	MSAVI + TVDI + Albedo	MSAVI + LST + TVDI	Albedo + TVDI + FVC	Albedo + LST + FVC
Classification precision (%)	90.23	89.18	86.84	88.52	87.67
Four indicators	MSAVI + Albedo + LST + TVDI			FVC + Albedo + LST + TVDI	
Classification precision (%)	93.83			92.05	
Five indicators	MSAVI + Albedo + LST + TVDI + FVC				
Classification precision (%)	95.21				

Table 4 Classification and indicators of desertification grades

Degree of desertification	Proportion of site (%)		Land surface characteristics
	Shifting sand	Vegetation cover	
Light	5	>60	Only small, sparse, scattered patches of mobile sand or wind-eroded areas are present; most parts of the area still resemble the original landscape. Vegetation occurs throughout the area, but some parts have suffered from degradation as a result of insufficient water or unsustainable human activity
Moderate	25	30	Mobile sand sheets, coppice dunes, and eroded land are present throughout the area. However, the eroded areas and mobile sand sheets are scattered and sparse. The vegetation cover is significant but is interspersed with sand sheets, sand dunes, or wind-eroded areas
Severe	50	10	Semi-anchored dunes cover most of the area, but some scattered mobile sand dunes or sand sheets are present around the semi-anchored sand dunes. Eroded areas or sand sheets are widely scattered throughout the area. There is sparse vegetation cover
Extremely	>50	<10	Dense, mobile sand dunes, or wind-eroded areas are widely distributed in the area. There is little or no vegetation

corrected using the FLAASH module of the ENVI 4.8 software (Agrawal et al. 2011). FLAASH is a first-principles atmospheric correction that incorporates the MODTRAN4 radiation transfer code to correct the wavelengths in the visible, near-infrared, and short-wave infrared bands up to 3 nm (Sun et al. 2010; Wang et al. 2010).

We used version of ENVI 4.8 software to create false-color images obtained by stacking data from the near-infrared, red, and green bands to perform geometrical correction. More details of the methods for satellite image processing are described by Navas and Machin (1997), Valle et al. (1998), and Vasconcelos et al. (2002). Our evaluation included both the area of desertified land and the degree of degradation. We classified the desertified land into five grades (Table 4). We used field surveys on August, and 35 sites had surveyed to determine the actual degree of desertification and then related the correlation analysis to the characteristics of TM and HJ images from the August of 2010 to determine the actual status of the desertified land using TM and HJ images. We determined the location of the field survey sites with a 2D precision of 4 m using a global positioning system and recorded land surface features using a digital camera. All images were interpreted manually using version ENVI 4.8 software and 9.1 of ArcGIS (<http://www.esri.com/software/arcgis>) according to the criteria in Table 4. In the last step, we created maps of the distribution of desertified using ArcGIS and compared them between periods to determine the dynamics of the temporal changes and spatial patterns of desertification between 2000 and 2010. To detect transfers among different desertification categories and produce a land transfer matrix, we used the graphical superposition method of Li et al. (2007).

We used this data to assess the dynamics of desertification. We used the following equation (Zhao et al. 2001):

$$D_i = ST_i/DI_i \times 1/T \times 100\% \tag{1}$$

where *i* is the degree of desertification, with 0 representing no desertification, versus 1 for light, 2 for moderate, 3 for severe, and 4 for extremely severe desertification; *D_i* is the

dynamic response of desertification of degree i ; DI_i is the area of the i th degree of desertification in the initial year of a study period; ST_i is the area of the i th degree of desertification that transferred to other grades of desertification during a study period; and T is the duration of the study period. The annual ratio of desertification was calculated using the following equation (Zhu and Chen 1994):

$$R_i = (\sqrt[T]{DI_i/AI_i} - 1) \times 100\% \quad (2)$$

where R_i is the annual ratio, and AI_i is the area of the i th degree of desertification after T years.

2.4 Meteorological and socioeconomic data

We collected and analyzed local meteorological and socioeconomic data to explore the mechanisms responsible for desertification. Meteorological data were obtained from four meteorological stations (Dunhuang, Jiuquan, Zhangye, and Wuwei) in the Hexi region. As proxies of human activity between 2000 and 2010, we chose the population in each year, livestock numbers (cattle, horses, camel, donkey, goats, and sheep), the area of cultivated land, and net primary productivity (NPP). We collected this data from the statistics departments of local governments and from the Gansu Development Yearbook (Gansu Development Yearbook). Thematic maps, geomorphologic maps, and vegetation maps (<http://westdc.westgis.ac.cn/>) were also used as supplementary data sources.

3 Results

3.1 Dynamic changes in the area of desertification from 2000 to 2010

Using the calculation method described in Sect. 2.2, we obtained weights of 0.30 for MSAVI, 0.25 for FVC, 0.20 for Albedo, 0.15 for LST, and 0.10 for TVDI. Figure 2 shows the spatial distribution of desertified land in the Hexi corridor in 2000, 2005, and 2010 based on the weighted sum of these indicators. The spatial distribution of the desertified land was similar in 2000, 2005, and 2010, with desertified land mainly distributed in the north and west, beside of oasis areas (cultivated land in Fig. 1) and bodies of water, and in regions with sand dunes (mobile dunes, semi-fixed dunes, and fixed dunes).

Table 5 shows the area of each degree of desertification and its corresponding proportion of the total land area in each of the three years. The total area included in our monitoring was $27.59 \times 10^4 \text{ km}^2$, and the total area of desertified land was 22.02×10^4 , 21.22×10^4 , and $21.06 \times 10^4 \text{ km}^2$ in 2000, 2005, and 2010, respectively, which amounted to 79.8, 76.9, and 76.3 % of the total area. Most of the desertified land was extremely severely desertified in each year. The lightly, moderately, severely, and extremely severely desertified land accounted for 0.71×10^4 , 1.55×10^4 , 3.89×10^4 , and $15.87 \times 10^4 \text{ km}^2$, respectively, of the total study area in 2000. However, the lightly, moderately, severely, and extremely severely desertified land accounted for 0.71, 1.38, 3.13, and $15.83 \times 10^4 \text{ km}^2$ of the total in 2010, respectively.

The area of land with no desertification increased at annual ratio was -2.65 and -0.62 % from 2000 to 2005 and from 2005 to 2010, respectively (Table 5). From 2000 to 2005, the areas of lightly, moderately, severely, and extremely severely desertified land decreased, with the largest decrease for severely and moderately desertified land, with

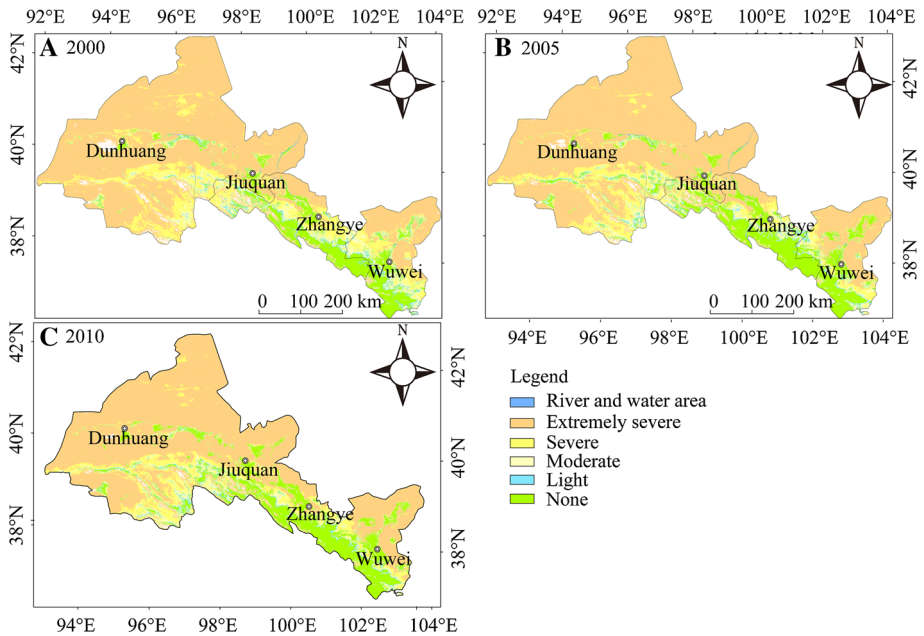


Fig. 2 Distribution of the desertified land in 2000, 2005, and 2010

values of 3.69 and 0.55 %, respectively. From 2005 to 2010, the areas of lightly and severely desertified land increased, by 0.03 and 0.14 %, respectively, but the areas of moderately and extremely severely desertified land decreased, by 0.10 and 0.80 %, respectively (Table 5).

3.2 Spatial changes, and transfers between different degrees of desertification

Based on change of the difference in the total desertification indicator between years, we defined five types of desertification pattern: strong development (−0.6 to −0.4), development (−0.4 to −0.2), stability (−0.2 to 0.2), reversal (0.2–0.4), and strong reversal (0.4–0.6). Figure 3 shows the spatial changes in desertification from 2000 to 2005 and from 2005 to 2010. In both periods, most of the study region showed a stability or reversal of desertification. From 2000 to 2005, the area that showed stability was largest ($17.77 \times 10^4 \text{ km}^2$), followed by the areas with a reversal of desertification ($1.53 \times 10^4 \text{ km}^2$), strong reversal ($0.95 \times 10^4 \text{ km}^2$), development ($0.16 \times 10^4 \text{ km}^2$), and strong development ($<0.01 \times 10^4 \text{ km}^2$). From 2005 to 2010, the area with stability was also the largest ($21.89 \times 10^4 \text{ km}^2$), followed by the areas with desertification development ($1.02 \times 10^4 \text{ km}^2$), reversal ($0.70 \times 10^4 \text{ km}^2$), strong reversal area ($0.18 \times 10^4 \text{ km}^2$), and strong development ($0.16 \times 10^4 \text{ km}^2$).

In 2005, the area of desertification decreased relative to that in 2000. Figure 3 shows that the reversal mainly occurred at the border of oasis areas and in the mountains. It is possible that rainfall increased in this region and that the rainfall was sufficient to support vegetation, but unfortunately, no meteorological stations provided data for most of these areas. However, the area of desertification development was mainly distributed in the southeastern region and between mountains and oasis areas. From 2000 to 2005, the area of

Table 5 Areas of desertified land in 2000, 2005, and 2010

Degree	2000		2005		2010		Annual ratio (%)	
	Area ($\times 10^4$ km ²)	Proportion of total (%)	Area ($\times 10^4$ km ²)	Proportion of total (%)	Area ($\times 10^4$ km ²)	Proportion of total (%)	2000–2005	2005–2010
None	5.57	20.19	6.37	23.09	6.53	23.81	-2.65	-0.62
Light	0.71	2.58	0.70	2.54	0.71	2.57	0.28	-0.28
Moderate	1.55	5.62	1.40	5.07	1.38	4.97	2.06	0.43
Severe	3.89	14.09	3.09	11.20	3.13	11.34	4.71	-0.26
Extremely severe	15.87	57.51	16.03	58.10	15.83	57.30	-0.20	0.28
Total	27.59	100	27.59	100	27.59	100		

Values may not total 100 % of the area due to rounding errors

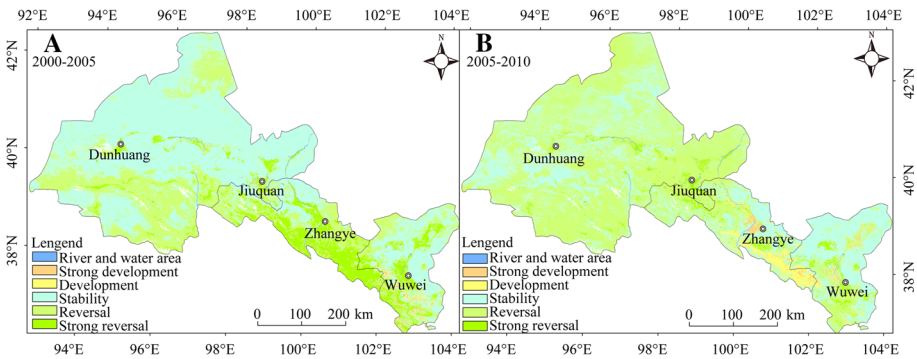


Fig. 3 Trends of desertification development from 2000 to 2005 and from 2005 to 2010

Table 6 Transfer matrix for land that changed between different degrees of desertification

Period	Initial degree ^a	Final degree ($\times 10^4 \text{ km}^2$)				
		L	M	S	ES	No
2000–2005	L	14.88	0.02	0.08	0.88	0.04
	M	0	0.1	0.1	0.06	0.43
	S	0.04	0.31	0.44	0.3	0.45
	ES	0.92	0.22	0.73	1.83	0.18
	No	0.18	0.06	0.05	0.02	
Total	Newly desertified: 0.31, reversal desertified: 1.10					
2005–2010	L	15.17	0.01	0.04	0.77	0.04
	M	0.01	0.19	0.16	0.07	0.28
	S	0.04	0.25	0.58	0.36	0.17
	ES	0.55	0.08	0.51	1.89	0.06
	No	0.08	0.15	0.08	0.04	
Total	Newly desertified: 0.35, reversal desertified: 0.55					

^a No, no desertification; L, light desertification; M, moderate desertification; S, severe desertification; ES, extremely severe desertification

desertified land increased by $0.31 \times 10^4 \text{ km}^2$, whereas desertification reversal occurred in $1.10 \times 10^4 \text{ km}^2$ (Table 6). More specifically, $0.45 \times 10^4 \text{ km}^2$ of severely desertified land changed to non-desertified land, and $0.18 \times 10^4 \text{ km}^2$ of non-desertified land change became lightly desertified land, accounting for 58.1 and 40.9 % of the total newly desertified land and reversal land, respectively.

In 2010, the area of desertified land also decreased relative to that in 2005. Figure 3 shows that the area in which reversal occurred was mainly distributed at the border of oasis areas, which because of the area of cultivated land decreased in this region (Sect. 4.2, Table 7). However, the area in which desertification developed was mainly distributed in the mountains, mainly because the snow area and the rainfall in the mountains decreased (Han et al. 2009). From 2005 to 2010, the area of desertified land increased by $0.35 \times 10^4 \text{ km}^2$, and the area where reversal occurred amounted to $0.55 \times 10^4 \text{ km}^2$ (Table 6). Moderate desertification changed to no desertification in $0.28 \times 10^4 \text{ km}^2$, whereas $0.15 \times 10^4 \text{ km}^2$ of non-desertified land changed to moderate desertification, accounting for 50.9 and 42.9 % of the desertified and reversal land, respectively.

Table 7 Dynamic response (D_i) of desertification during the two periods

	Degree ^a				
	No	L	M	S	ES
2000–2005	17.45	20.40	22.13	25.18	19.81
2005–2010	19.55	19.76	20.26	19.71	20.23
Average	18.50	20.08	21.19	22.45	20.02

^a No, no desertification; L, light desertification; M, moderate desertification; S, severe desertification; ES, extremely severe desertification

3.3 Desertification dynamics in land with different degrees of desertification

Between 2000 and 2010, the area of desertified land decreased by 1.0×10^4 km², for an annual transformation rate of -3.25 %, and this decrease was almost the same as increase in the area of newly desertified land (0.96×10^4 km²). Table 7 shows the dynamic response of desertification during the two periods. From 2000 to 2005, the greatest dynamic response (D_i) was in land with severe desertification (25.2 %), followed by land with moderate, light, extremely severe, and no desertification. However, from 2005 to 2010, the greatest dynamic response was in land with moderate desertification (20.3 %) and then extremely severe, light, severe, and no desertification. From 2000 to 2010, the averaged dynamic response was largest for land with severe desertification (22.4 %), followed by moderate, light, extremely severe, and no desertification.

4 Discussion

Many factors can contribute to the observed desertification dynamics; these include climate, soil, vegetation, socioeconomic changes, and human activities. We summarized these variables as natural factors and human activities, each of which had different contributions to desertification processes.

4.1 Climate factors

Climate change is an important driving force for desertification in China (Zhu and Liu 1989; Wang et al. 2006). Climate affects on desertification mainly through its influence on air temperature, precipitation, relative humidity, and so on. Changes in air temperature, precipitation, relative humidity, and wind velocity change the threshold wind velocity for eolian entrainment of soil particles. High temperatures, low precipitation, and high wind velocity will exacerbate desertification. In this study, we used data from four meteorological stations to analyze the climate changes in our study area. We analyzed the air temperature, precipitation, relative humidity, and annual number of sandstorm days to represent climatic changes during the study period. We used linear regression ($y = a + bx$) to identify trends in these four parameters (Supplement Table S1). The mean annual temperature increased at all four stations, by an average of 0.6 °C from 2000 to 2010, and increased most strongly at the Zhangye station ($R^2 = 0.57$), by 1.1 °C (Fig. 4). Because increased air temperature could increase evaporation and decrease soil moisture content, leading to decreased vegetation cover and increased wind erosion, this trend

Fig. 4 Changes in four key climatic parameters from 2000 and 2010 at Zhangye weather stations in the study area

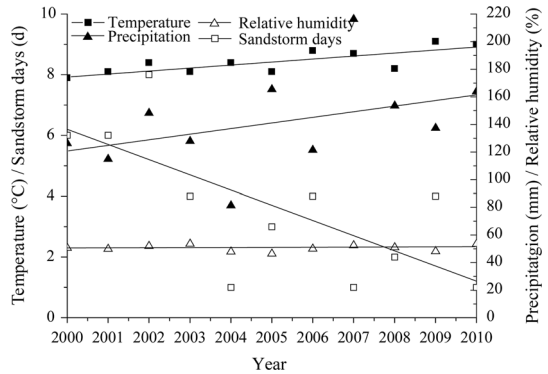


Table 8 Comparison of desertification land in two periods relative to the proxies of human activities

	Population ($\times 10^4$)	NPP ($\times 10^4 \text{ g a}^{-1}$)	Livestock ($\times 10^7$)	Cultivated land ($\times 10^6$)	Desertification area ($\times 10^4 \text{ km}^2$)
2000–2005	19.94	8.10	3.01	0.19	−0.82
2005–2010	−15.81	0.61	2.14	−0.11	−0.17

indicates greater potential risk of desertification. The precipitation and relative humidity showed similar trends at all four sites; however, at Dunhuang and Wuwei, the precipitation and relative humidity decreased, whereas both increased at Jiuquan and Zhangye. The precipitation increased most strongly at the Wuwei station ($R^2 = 0.17$), and the relative humidity increased most strongly at the Zhangye station ($R^2 = 0.43$). The number of sandstorm days decreased at all four stations and decreased most strongly at the Wuwei station ($R^2 = 0.35$). This factor would tend to indicate a decreased risk of desertification in all four areas.

4.2 Human activities

Desertification is also the result of human factors. Human activities such as population growth, overgrazing, and overcutting of vegetation could increase desertification, whereas offsetting activities such as planting vegetation and various techniques to combat desertification could decrease desertification. In this paper, we evaluated human activities using four proxies: the human population, the number of livestock, the area of cultivated land, and changes in NPP, which we used as an indication of changes in vegetation cover (Table 8).

The region’s population increased by 19.94×10^4 from 2000 to 2005 and decreased by 15.81×10^4 from 2005 to 2010 as a result of the implementation of an ecological migration policy imposed by the central government, which had the goal of moving residents to areas with a less fragile environment and higher carrying capacity. The increased population led to urban expansion and increased intensity of human activities, including an increased area of cultivated land and destruction of natural vegetation. Both factors would tend to promote desertification, as would grazing. In the oasis areas, increased populations combined with irrational land usage and overexploitation of water sources to increase the risk of desertification.

The livestock number increased by 3.01×10^7 and 2.14×10^7 from 2000 to 2005 and 2005 to 2010, respectively. More livestock need more grassland, and the resulting overgrazing destroyed grassland and exposed the top layer of the soil to wind erosion and nutrient loss that reduced the growth of the remaining vegetation. The government prohibited grazing in many areas to combat this process, leading to decreased livestock numbers, allowing the grassland to recover, and leading to reversal of desertification.

The area of cultivated land increased by $0.19 \times 10^4 \text{ km}^2$ from 2000 to 2005 and decreased by $0.11 \times 10^4 \text{ km}^2$ from 2005 to 2010. These changes corresponded to the aforementioned population changes, leading to increased reclamation of land for agriculture from 2000 to 2005 and an increased risk of desertification. However, from 2005 to 2010, the decreased population led to the abandonment of cultivated land, thereby decreasing pressure on the desertified land and allowing it to recover.

Kang et al. (2004) concluded that overexploitation and overutilization of water resources in the artificial oases in the middle reaches in three inland river basins have caused degradation of the ecological environment, leading to desertification of the natural oases in downstream reaches. The water resource problems related to desertification in the Shiyang River Basin, including competition for water resources among users in the upper, middle, and downstream parts of the basin, have increased the degradation of natural oases and increased desertification in downstream regions (Fang and Sun 2006; Dong 2009; Xie 2004; Du et al. 1996).

Recently, a series of key national projects have been initiated to combat desertification in the study area. These include the Three Norths Shelterbelt Project, the Conversion of Cropland to Forest or Grassland Program, and the Water and Soil Conservation Program (Xue et al. 2013). Under these programs, the NPP increased in $8.10 \times 10^4 \text{ g a}^{-1}$ of the study area from 2000 to 2005 and in $0.61 \times 10^4 \text{ g a}^{-1}$ of the study area from 2005 to 2010 (Table 8). The change of NPP directly reflects the desertification process. From 2000 to 2005, NPP increases more than it did during 2005 to 2010, leading to a greater reversal of desertification from 2000 to 2005 ($0.82 \times 10^4 \text{ km}^2$) than from 2005 to 2010 ($0.17 \times 10^4 \text{ km}^2$). Although the increase in NPP was greater in the first period, the ecological migration policy compensated for this somewhat by greatly decreasing human pressure on the land.

In our study area, the area in which reversal of desertification occurred responded to the observed changes in the population, livestock number, and vegetation cover (Table 8). Therefore, human factors were strong contributors to desertification.

5 Conclusions

We used remote-sensing imagery to calculate five indicators of desertification and monitor its spatial and temporal pattern in the Hexi corridor of northern China from 2000 to 2010. The area affected by significant desertification in the Hexi corridor was large, amounting to more than 76 % of the total land area. From 2000 to 2010, desertified land decreased by $0.06 \times 10^4 \text{ km}^2$, at an annual rate of 0.90 %. From 2000 to 2005 and from 2005 to 2010, most of the area of desertified land showed either a stability or reversal of desertification. Both natural and human factors contributed to the desertification dynamics during the study period. The trends in several natural factors contributed to a reversal of desertification in some areas. However, human factors such as population changes and increased cultivation of land appear to have been stronger driving forces that were directly responsible for the changes in desertification. Several national projects are currently

underway to reverse desertification, and the present results show that it should be possible to monitor the effects of these policies by means of remote sensing.

Acknowledgments We gratefully acknowledge funding from the National Natural Science Foundation of China (41101007), National Key Research and Development (973) Program of China 2013CB430200 (2013CB430206), the Natural Science Foundation of Gansu Province's Youth Science and Technology Foundation Project (1208RJYA027) and the key research project of the Gansu Provincial Meteorological Bureau (2010-08 and 2012-11).

References

- Adamo SB, Crews-Meyer KA (2006) Aridity and desertification: exploring environmental hazards in Jáchal, Argentina. *Appl Geogr* 26:61–85
- Agrawal G, Bhopal M, Sarup J (2011) Comparison of QUAC and FLASSH atmospheric correction modules on EO-1 hyperion data of Sanchi. *Int J Adv Eng Technol* 4:178–186
- Arnalds A (2004) Desertification in a humid environment: an example from Iceland. *Encyclopedia of soil science*, Taylor & Francis, p 6
- China National Committee for the Implementation of the UNCCD (CCICCD) (2006) China National Report on the Implementation of the United Nation's Convention to Combat Desertification. Beijing (in Chinese)
- Dall-Olmo G, Karnieli A (2002) Monitoring phenological cycles of desert ecosystems using NDVI and LST data derived from NOAA-AVHRR imagery. *Int J Remote Sens* 23(19):4055–4071
- Ding H, Chen J, Wang G (2009) A model for desertification evolution employing GIS with cellular automata. In: International conference on computer modeling and simulation, Macau, China, 20–22 Feb 2009. IEEE 2009, pp 324–328
- Dong PH (2009) Evaluation on the water-land resource of space layout and constitution in Gansu Province. *Arid Land Geogr* 32(6):834–840 (in Chinese)
- Dregne H, Kassas M, Rozanov B (1991) A new assessment of the world status of desertification. *Desertif Control Bull* 20:6–18
- Du HL, Gao QZ, Li FX (1996) Trend analysis of surface water resource and dynamics in the interior drainage basins of Hexi area. *Resour Sci* 2:44–54 (in Chinese)
- Fang CL, Sun XL (2006) Mechanism of urban system development and its space organization in northwest arid area with scarcity of water resource—the case of Hexi Corridor. *J Desert Research* 26(5):860–868 (in Chinese)
- Gansu Development Yearbook (2013) China Statistics Press, Beijing (in Chinese)
- Gao ZH, Ding F, Wei HD (2001) Actualities, cause and control of desertification in Hexi Region, Gansu Province. *J Nat Disasters* 10(4):70–75 (in Chinese)
- Ge XD, Ni JR, Li ZS, Hu RG, Ming X, Ye Q (2013) Quantifying the synergistic effect of the precipitation and land use on sandy desertification at county level: a case study in Naiman Banner, northern China. *J Environ Manage* 123:34–41
- Geist HJ, Lambin EF (2004) Dynamic causal patterns of desertification. *Bioscience* 54:817–829
- Han Z (2003) The evolution of the Mao wusu Desert and the reclamation in the adjacent areas in the Ming Dynasty. *China Soc Sci* 5:191–204
- Han LY, Han T, Zhang ZC, Liang Y, Li MX (2009) Water resource and ecological environment remote sense monitor analysis over 10 years in Shiyanghe River Basin. *Pratac Sci* 10:46–51
- Han LY, Wan X, Fang F, Zhang ZC (2013) Desertification assessments of Hexi regions in Gansu province by remote sensing. *Arid Land Geogr* 36:131–138
- Han XX, Chen XL, Qin C, Feng L, Tian LQ (2014) Study on drought monitoring based on HJ-1A/1B image case of Panyanglake watershed. *J Huazhong Normal Univ (Nat Sci)* 48:274–278
- Hu GY, Dong ZB, Lu JF, Yan CZ (2012) Driving forces responsible for aeolian desertification in the source region of the Yangtze River from 1975 to 2005. *Environ Earth Sci* 66:257–263
- Kang ES, Li X, Zhang JS, Hu XL (2004) Water Resources Relating to Desertification in the Hexi Area of Gansu Province, China. *J Glaciol Geocryol* 26(6):657–667 (in Chinese)
- Kassas M (1995) Desertification: a general review. *J Arid Environ* 30:115–128
- Li BL, Zhou CH (2001) Sandy desertification in west of Northeast China Plain in the past 10 years. *Acta Geogr Sin* 56(3):307–315 (in Chinese)

- Li S, Zheng Y, Luo P, Wang X (2007) Desertification in western Hainan Island, China (1959 to 2003). *Land Degrad Dev* 18:473–485
- Li ZG, Wang YL, Zhou QB, Wu JS, Peng J, Chang HF (2008) Spatiotemporal variability of land surface moisture based on vegetation and temperature characteristics in Northern Shaanxi Loess Plateau, China. *J Arid Environ* 72(6):974–985
- Li JY, Yang XC, Jin YX, Yang Z, Huang WG, Zhao LN, Gao T, Yu HD, Ma HL, Qin ZH, Xu B (2013) Monitoring and analysis of grassland desertification dynamics using Landsat images in Ningxia, China. *Remote Sens Environ* 138:19–26
- Liu SL, Wang T (2007) Aeolian desertification from the mid-1970s to 2005 in Otindag Sandy Land, Northern China. *Environ Geol* 51:1057–1064
- Liu Y, Gao J, Yang Y (2003) A holistic approach towards assessment of severity of land degradation along the Great Wall in northern Shaanxi province, China. *Environ Monit Assess* 82:187–202
- Luo F, Qi SZ, Xiao HL (2005) Landscape change and sandy desertification in arid areas: a case study in the Zhangye Region of Gansu Province, China. *Environ Geol* 49:90–97
- Luo JH, Zhang JC, Huang WJ, Yang GJ, Gu XH, Yang H, Huang WJ (2010) The analysis of consistency between HJ-1 B and Landsat 5 TM for retrieving LST based on the single-channel algorithm. *Spectrosc Spectr Anal* 30(12):3285–3289
- Ma JH, Xiao T (2007) Qualified evaluating on the remote sensing of desertification—a case study of the Erdos region. *J Lanzhou Univ (Nat Sci)* 43(4):1–6 (in Chinese)
- Ma JZ, Wang XS, Edmunds WM (2005) The characteristics of groundwater resources and their changes under the impacts of human activity in the arid Northwest China—a case study of the Shiyang River Basin. *J Arid Environ* 61:277–295
- Middleton N, Thomas DSG (1997) world atlas of desertification. Edward Arnold, London
- Nasrallah HA, Balling RCJ (1993) Spatial and temporal analysis of Middle Eastern temperature changes. *Clim Change* 25:153–161
- Navas A, Machin J (1997) Assessing erosion risk in the gypsiferous steppe of Litigio (NE Spain). An approach using GIS. *J Arid Environ* 37:433–441
- Niu BR (2005) Study on quantitative extraction of desertification degree information from remote sensing information. *J Catastrophol* 20(1):18–21
- Salvati L, Zitti M, Ceccarelli T (2008) Integrating economic and environmental indicators in the assessment of desertification risk: a case study. *Appl Ecol Environ Res* 6:129–138
- Santini M, Caccamo G, Laurenti A, Noce S, Valentini R (2010) A multi-component GIS framework for desertification risk assessment by an integrated index. *Appl Geogr* 30:394–415
- Shalaby A, Tateishi R (2007) Remote sensing and GIS for mapping and monitoring land cover and land-use changes in the Northwestern coastal zone of Egypt. *Appl Geogr* 27:28–41
- Shi JZ, Chen XS, Zhang LS, Li XB, Wei JP (2006) The condition and changing trend analysis of desertification land in Gansu Province. *Acta Sci Circumst* 26(9):1539–1544 (in Chinese)
- Sivakumar MVK (2007) Interactions between climate and desertification. *Agric For Meteorol* 142:143–155
- Sun L, Sun C, Liu Q, Zhong B (2010) Aerosol optical depth retrieval by HJ-1/CCD supported by MODIS surface reflectance data. *Sci China Earth* 53:74–80
- UNCCD (1994) Elaboration of an international convention to combat desertification in countries experiencing serious drought and/or desertification and particular in Africa. Final negotiations text of the convention. Unites Nations, Geneva
- Valle HF, Elissalde NO, Gagliardini DA, Milovich J (1998) Status of desertification in the Patagonian Region: assessing and mapping from satellite imagery. *Arid Soil Res Rehabil* 12:95–122
- Vasconcelos M, Mussa-Biai JC, Araujo A, Diniz M (2002) Land cover changes in two protected areas of Guinea-Bissau (1956–1998). *Appl Geogr* 22:139–156
- Wang T (2003) Desert and aeolian desertification in China. Science Press, Beijing (in Chinese)
- Wang T, Zhu ZD (2003) Study on sandy desertification in China—I. Definition of sandy desertification and its connotation. *J Desert Res* 3:209–214 (in Chinese)
- Wang T, Wu W, Wang XZ (1998) Remote sensing monitoring and assessing sandy desertification: an example from the sandy desertification region of northern China. *Quat Sci* 2:108–118 (in Chinese)
- Wang JH, Zhang LS, Shang LZ (2005) Desertification monitoring and its result in Gansu Province. *J Desert Res* 25(5):775–779 (in Chinese)
- Wang XM, Chen FH, Dong ZB (2006) The relative role of climatic and human factors in desertification in semiarid China. *Glob Environ Change* 16:48–57
- Wang XM, Cheng FH, Hasi E, Li JC (2008) Desertification in China: an assessment. *Earth Sci Rev* 88:188–206
- Wang Q, Wu C, Li Q, Li J (2010) Chinese HJ-1A/B satellites and data characteristics. *China Earth Sci* 53:51–57

- Wang CT, Zhang YJ, Qian ZQ, Chen JX, Cao M (2013a) Surface Albedo estimating based on HJ-1B/CCD. *Geogr Geo-Inf Sci* 29:12–16
- Wang HY, Li XS, Zhang J, Gao ZH (2013b) Accuracy comparison of BJ-1, HJ and Landsat data in the retrieval of grassland vegetation coverage, leaf area index and above ground biomass. *Spectrosc Spectr Anal* 10:2803–2808
- Wu W (2001a) Using the TM image for monitoring land desertification. *J Desert Res* 16(2):86–90 (in Chinese)
- Wu W (2001b) Study on desertification process in Mu Us sand land for last 50 years, China. *J Desert Res* 21(2):164–169 (in Chinese)
- Xie JZ (2004) Water resources problems and water-saving strategies in Hexi Corridor. *J Desert Res* 24(6):802–808 (in Chinese)
- Xu DY, Li C, Zhuang D, Pan JJ (2011) Assessment of the relative role of climate change and human activities in desertification: a review. *J Geogr Sci* 21:926–936
- Xue ZJ, Qin ZD, Li HJ, Ding GW, Meng XW (2013) Evaluation of aeolian desertification from 1975 to 2010 and its causes in northwest Shanxi Province, China. *Glob Planet Change* 107:102–108
- Zeng YN, Feng ZD (2007) Spatial and temporal changes of desertification in the headwater area of the Yellow River using remote sensing. *Acta Geogr Sin* 62(5):529–536 (in Chinese)
- Zeng YN, Xiang NP, Feng ZD, Xu H (2006) Albedo-NDVI space and remote sensing synthesis index models for desertification monitoring. *Sci Geogr Sin* 26(1):75–81 (in Chinese)
- Zhang SB (2007) Research on the eco-system degradation and rehabilitation of Hexi corridor in Gansu Province. Northwest A & F University, Yangling (in Chinese)
- Zhang YZ, Chen ZY, Zhu BQ, Luo XY, Guan YN, Guo S, Nie YP (2008) Land desertification monitoring and assessment in Yulin of Northwest China using remote sensing and geographic information systems (GIS). *Environ Monit Assess* 147:327–337
- Zhao J, Wei CJ, Huang LF (2001) Research methods of land use changes and their applications in Hainan Island. *Geogr Res* 20(6):723–730 (in Chinese)
- Zhu ZD, Chen GT (1994) *Sandy desertification China*. Science Press, Beijing (in Chinese)
- Zhu ZD, Liu S (1989) *Desertification and its governance in China*. Science Press, Beijing (in Chinese)